

**High Efficient Photovoltaic Devices
Fabricated from Self-Assemble Block
Insulating-Conducting Copolymer Containing
Semiconducting Nanoparticles**

Contract No. FA5209-04-P-0500, AOARD04-23
Period: 2004/08/05~2005/08/04

Principle Investigator: Wei-Fang Su
Coinvestigator: L-Y Wang, C-A Dai, C-W Chen

National Taiwan University

Report Documentation Page

Form Approved
OMB No. 0704-0188

Public reporting burden for the collection of information is estimated to average 1 hour per response, including the time for reviewing instructions, searching existing data sources, gathering and maintaining the data needed, and completing and reviewing the collection of information. Send comments regarding this burden estimate or any other aspect of this collection of information, including suggestions for reducing this burden, to Washington Headquarters Services, Directorate for Information Operations and Reports, 1215 Jefferson Davis Highway, Suite 1204, Arlington VA 22202-4302. Respondents should be aware that notwithstanding any other provision of law, no person shall be subject to a penalty for failing to comply with a collection of information if it does not display a currently valid OMB control number.

1. REPORT DATE 14 DEC 2005		2. REPORT TYPE FInal		3. DATES COVERED 05-08-2004 to 05-08-2005	
4. TITLE AND SUBTITLE High Efficiency Photovoltaic Devices Fabricated from Self- Assemble Block Insulating-Conducting Copolymer Containing				5a. CONTRACT NUMBER FA520904P0500	
				5b. GRANT NUMBER	
				5c. PROGRAM ELEMENT NUMBER	
6. AUTHOR(S) Wei-Fang Su				5d. PROJECT NUMBER	
				5e. TASK NUMBER	
				5f. WORK UNIT NUMBER	
7. PERFORMING ORGANIZATION NAME(S) AND ADDRESS(ES) National Taiwan University,1, Roosevelt Road Sec. 4,Taipei 106,Taiwan,TW,106				8. PERFORMING ORGANIZATION REPORT NUMBER N/A	
9. SPONSORING/MONITORING AGENCY NAME(S) AND ADDRESS(ES) AOARD, UNIT 45002, APO, AP, 96337-5002				10. SPONSOR/MONITOR'S ACRONYM(S) AOARD	
				11. SPONSOR/MONITOR'S REPORT NUMBER(S) AOARD-044023	
12. DISTRIBUTION/AVAILABILITY STATEMENT Approved for public release; distribution unlimited					
13. SUPPLEMENTARY NOTES					
14. ABSTRACT The contractor shall investigate novel self-assembled block insulating-conducting copolymers containing semiconducting nanoparticles for high efficiency photovoltaic devices					
15. SUBJECT TERMS Nanotechnology, PowerMEMS, Solar Cells					
16. SECURITY CLASSIFICATION OF:			17. LIMITATION OF ABSTRACT Same as Report (SAR)	18. NUMBER OF PAGES 24	19a. NAME OF RESPONSIBLE PERSON
a. REPORT unclassified	b. ABSTRACT unclassified	c. THIS PAGE unclassified			

High Efficient Photovoltaic Devices Fabricated from Self-Assemble Block Insulating-Conducting Copolymer Containing Semiconducting Nanoparticles

Executive Summary

We are developing aromatic based conducting polymer incorporation with nanoparticle to have high thermal stability and broad solar spectra absorption. The MEHPPV-CdSe hybrid was used as our control system. Temperature dependent steady-state and time resolved photoluminescence experimental studies of MEHPPV-CdSe reveals that the role of nanoparticles not only provides medium for efficient charge separation at the interface but also leads to the increase the effective conjugation length in the polymer, which could be beneficial for hole transport within the polymer chain.

We have demonstrated a synthetic route for preparing a novel hybrid materials of poly(3-hexylthiophene)/D-A linker/TiO₂. The chemical structure of the D-A linker which was used to chemically connect organic and inorganic phases was designed to contain three main parts: triethoxysilane group, alkyl spacer, and polymerizable thiophene ring. After the formation of self-assembled monolayers (SAMs) of linker on TiO₂ surface, the terminal thiophene ring in the linker was used as an initiation point to grow poly(3-hexylthiophene) chains electrochemically for fabricating the novel composite of poly(3-hexylthiophene)/D-A linker/TiO₂. Compared with neat P3HT films on TiO₂, it is interesting to note that the presence of the D-A linker between P3HT and TiO₂ effectively increase quenching of the photoluminescence.

The 3nm x 30nm TiO₂ nanorods were synthesized by modified sol-gel method under low temperature (90°C) and are in anatase structure. The TiO₂ nanorods/MEH-PPV hybrid material is fabricated for photovoltaic applications via spin coating process. The large interfacial area between the two materials due to high surface to volume ratio of rod shape nanocrystals ensures a more efficient charge separation. The material composed of 1-D nanostructure could potentially improve charge transport in photoactive materials. The photoluminescence was quenched by mixing CdSe nanoparticles with TiO₂. The results indicate the electron transport should be efficient in the blend nanoparticle system.

Patterning nanoparticles in self-assembled conducting/insulating block copolymers are under development to achieve high efficient charge separation and transport via increased interfacial interactions and reduced transport path between electrodes. Poly (*para*-phenylene)-b-Poly (2-vinyl pyridine) (PPP-PVP) were synthesized by using sequential anionic polymerization to produce a precursor of PPP-PVP, poly (1,3 cyclohexadiene)-b-poly (2-vinyl pyridine) (PCHD-PVP). PCHD-PVP copolymers were subsequently derivatized through an aromatization reaction and reduced to PPP-PVP. Different morphologies e.g. lamellae, cylinders and spheres of copolymers were fabricated. Semiconducting nanoparticles of cadmium sulfide (CdS) was incorporated into PPP-PVP nanostructure using in-situ synthesis of CdS in the PVP domain. Optoelectronic property of the CdS-PPP-PVP showed decreasing in bandgap and quenching in PL as compared with PPP-PVP. The results indicate the material can absorb solar energy more efficiently and increase the charge transport in the device. New copolymer system based on polythiophene is under development to improve the charge mobility of poly-p-phenylene copolymer system. Poly(3-hexylthiophene)-b-poly(2-vinylpyridine) was synthesized using sequential anionic polymerization. Their properties and morphology are currently under investigation.

Keywords: polymer, copolymer, conducting, nanoparticle, hybrid, photovoltaic, self-assembly, in-situ, photocurrent, mechanism.

Introduction

There has been an ever-increasing interest in the development of high efficiency and long life photovoltaic devices using renewable and clean solar energy. Although Si-based photovoltaic devices can harvest up to as much as 25% of the incoming solar energy, they are opaque and costly to make. On the contrary, recent progress in the development of conducting polymers has created the possibility of making transparent, light weight, low cost, flexible and large area photovoltaic devices. However, most polymer photovoltaic devices suffer from low efficiency in solar energy conversion and poor thermal stability. For many conducting polymers, electron mobilities are extremely low, and the photo-generated charges lose via recombination. A second material such as nanoparticle incorporated in conjugated polymer provides interface for charge separation and transport could overcome these problems. At present, the nanoparticle/polymer composites for photovoltaic devices are prepared by blending the semiconducting nanoparticle with conducting polymer in solvent. The nanoparticles are randomly distributed in the polymer matrix. In order for the nanoparticles in the polymer matrix to form a highly connected network, usually the nanoparticles have to be in high concentration. Problems of coagulation often occurs from high concentration of nanoparticles and reduce the interfacial interactions between the polymer and nanoparticle which results in decreasing quantum efficiency. Currently, the highest reported power conversion efficiency of polymer-nanoparticle photovoltaic device is an order lower than that of Si based material about 2.5~5%.¹

We work on a three year project with four subprograms using molecular design and molecular modeling concepts to manipulating chemical structures and compositions, size and organization of nanodomain, and interfacial interactions between inorganic nanoparticles and conducting polymers to form novel polymer-nanoparticle hybrid materials. They are investigated as active materials for the fabrication of high efficient and long life photovoltaic devices. Three strategies are used to achieve the objective: (1) using thermal stable materials having capability to absorb full solar spectra, (2) increasing interface between polymers and nanoparticles and (3) controlling mechanisms of charge separation and transport.

In the subprogram 1, we are developing thermal stable and high charge mobility nanoparticles with capability to absorb full solar spectra. The nanoparticles should be low bandgap thermal resistant oxide based material. In the subprogram 2, we are developing conducting polymer/nanoparticle donor/acceptor hybrid materials. They are designed to shorten the diffusion-length of excitons, to increase the interfacial areas and to improve the compatibility between polymer and nanoparticles. The materials will be synthesized using surface-initiated polymerization method and apply them to fabricate photovoltaic devices as an active material. In the subprogram 3, we are developing self-assemble hybrids of insulating/conducting block copolymers containing semiconducting nanoparticles. The block copolymers can self-assemble into highly ordered three dimensional structures. Since most semiconducting nanoparticles are hydrophilic, they can preferentially segregate into the hydrophilic/polar domain of the three dimensional network created by the block copolymer. The resulting interconnected 3D structure consisting of electron accepting conducting polymer domain and electron donating nanoparticles domain has substantially large interface for effective charge separation. In subprogram 4, we are exploring the nature of charge separation and carrier transport in the materials prepared in the project in terms of experimental and theoretical approaches.

In the first year, we have set up the laboratories for material synthesis, photovoltaic device fabrication and measurement. We demonstrated the PV conversion efficiency of hybrid MEHPPV-CdS system increased by 64 times as compared with that of pure polymer MEHPPV.

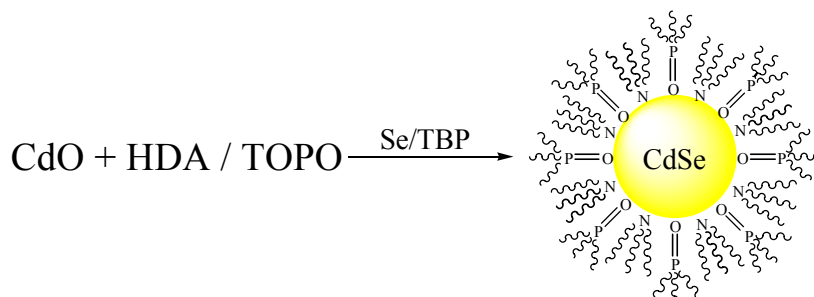
The second year progress of this program is reported in the following sections.

Subprogram 1 Synthesis of semiconducting nanoparticle

We have synthesized II-VI semiconductor nanoparticles, TiO₂ nanorods and a blend of CdSe and TiO₂ system.

II-VI semiconductor nanoparticles

According to Talapin² (2001), we synthesized CdSe nanoparticles in a mixed TOPO (Trioctylphosphine oxide) /HDA (Hexadecylamine) solvent and used CdO, complexed by HDA, as cadmium precursor at 320°C (Scheme 1). Then we cooled the solution to reaction temperature, 260 °C. At this temperature, the Se solution containing Se powder dissolved in TBP (Tri-n-butylphosphine) and was quickly injected into the reaction flask. By controlling the reaction time and temperature, different sizes of CdSe nanoparticles were synthesized successfully.



Scheme 1. Synthesis of CdSe nanoparticles

Figure 1 shows XRD patterns of CdSe nanocrystals. As expected, the width of the diffraction peaks is considerably broadened and increases with decreasing particle size. Nanocrystals exhibit XRD patterns with diffraction peaks in accord with those of hexagonal CdSe (wurtzite phase).

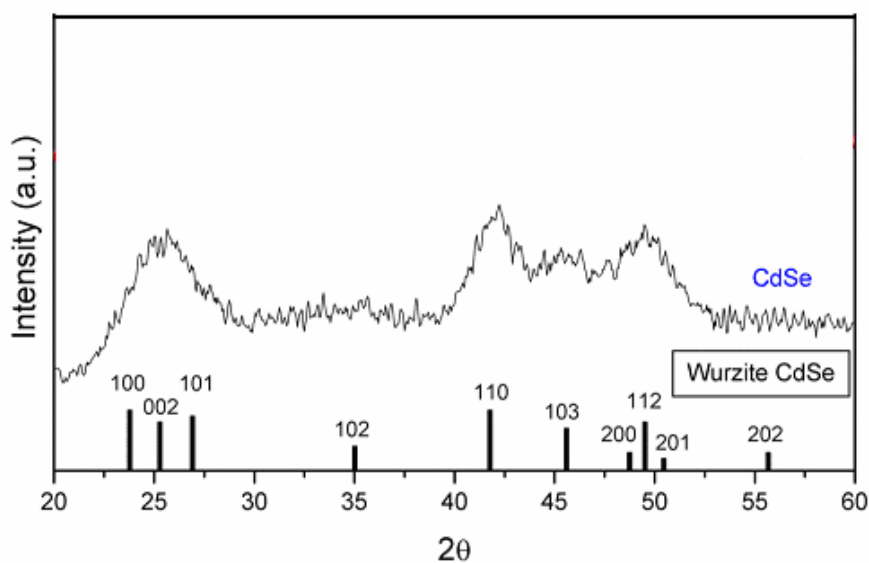
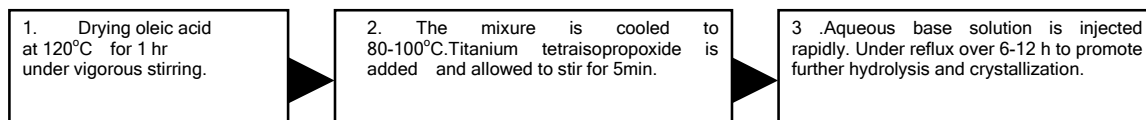


Figure 1. XRD patterns of CdSe nanocrystals

TiO₂ Nanorods

We have successfully synthesized TiO₂ nanorods. The oleic acid end-capped TiO₂ nanorods were synthesized by hydrolysis of titanium tetraisopropoxide (Scheme 2).



Scheme 2. Flow Diagram of TiO₂ nanorod synthesis

The length of TiO₂ nanorods was controlled by controlling of the acidity and concentration of reactants added. The nanorods synthesized are approximately 3-4nm in diameter, and an average of ~40nm in length, ~20nm and 4-10nm respectively. The structure characterization of TiO₂ nanorods was performed by powder X-ray diffraction (Figure 2).

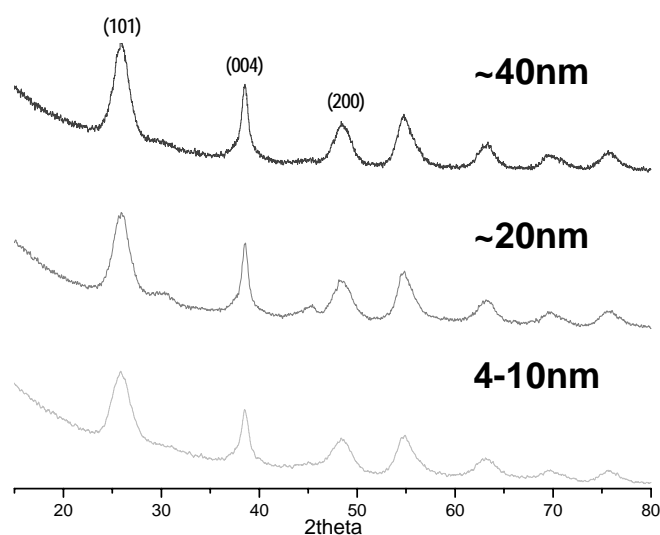


Figure 2. XRD patterns of TiO₂ nanorods

The nanocrystals were nearly perfect anatase with an extended crystalline domain in the (004) direction. We compared the intensity of (004) to that of standard TiO₂ sample and found that the relative intensity of (004) had increased. From the XRD pattern, characteristic lengths calculated with the Scherrer formula from the (101) peaks are ~4.5nm in three samples.

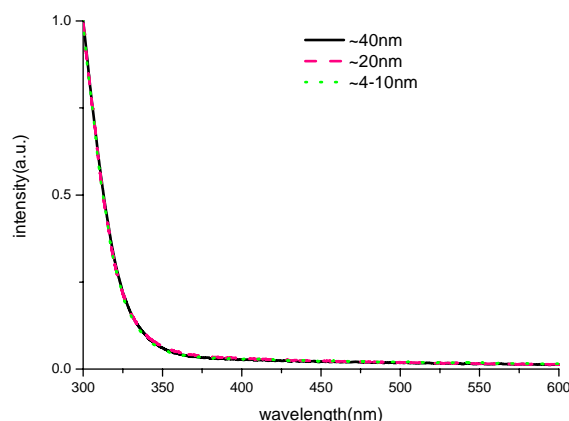


Figure 3. Absorption spectrum of nanorods

The absorption spectra of different sizes of TiO₂ nanorods were shown in Figure 3. Compared with the absorption onset data to the standard anatase, the size-quantization of the TiO₂ nanorods was not observed in three samples. This result is consistent with the size quantization of TiO₂, which occurs in the range of 0.75-1.9nm. The band gap of three samples are approximately the same.

Blend of CdSe/TiO₂

We have studied the effect of TiO₂ on the photo properties of CdSe nanoparticles by fabricating CdSe nanoparticles/TiO₂ spin-coatable film. Precursors of the titanium dioxide such as Ti-(OB_u)₄ are very reactive compounds because of the presence of electronegative alkoxy groups, making the metal atoms highly prone to nucleophilic attack. Due to the high affinity of Ti(OB_u)₄ to water, the hydrolysis reaction results in the formation of molecular aggregates of hydrated titanium oxide alkoxides. Controlling the hydrolysis rate of titanium precursor was a key point of the spin-coatable film. We used α -diketone BzAc to complex with Ti(OB_u)₄ to control the hydrolytic reactivity. The BzAc is capable of keto-enol tautomerism³, as shown in eq 1. The enol form of BzAc is stabilized by chelation with Ti(OB_u)₄. Further, the reaction also results in the partial replacement of the alkoxy group by α -diketonato ligand, as shown in eq 2. The hydrolytic activity of stabilized Ti(OB_u)₄ is substantially reduced-perhaps due to the steric hindrance. Equimolar amounts of Ti(OB_u)₄ and BzAc were reacted in methyl alcohol for 2 h at room temperature. The spin coating solution was formed by mixing the titanium alkoxide solution with CdSe nanoparticles solution. Emission spectra of CdSe nanoparticles solution and the hybrid solution were illustrated in Figure 4. The photoluminescence of CdSe nanoparticles was quenched by titanium alkoxide due to the charge transfer from the CdSe to TiO₂. The results should be useful to fabricate high efficiency solar cell.

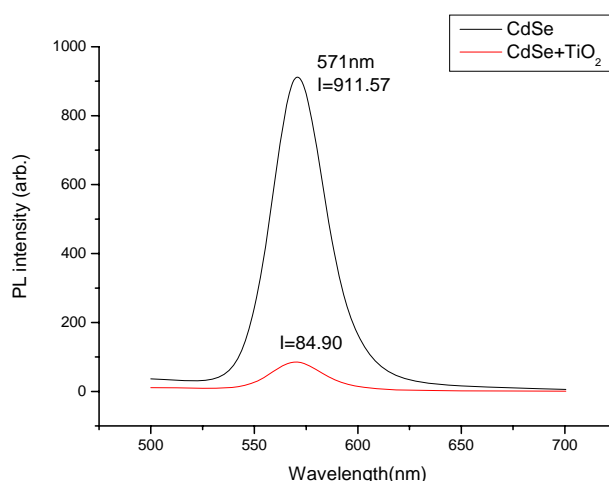
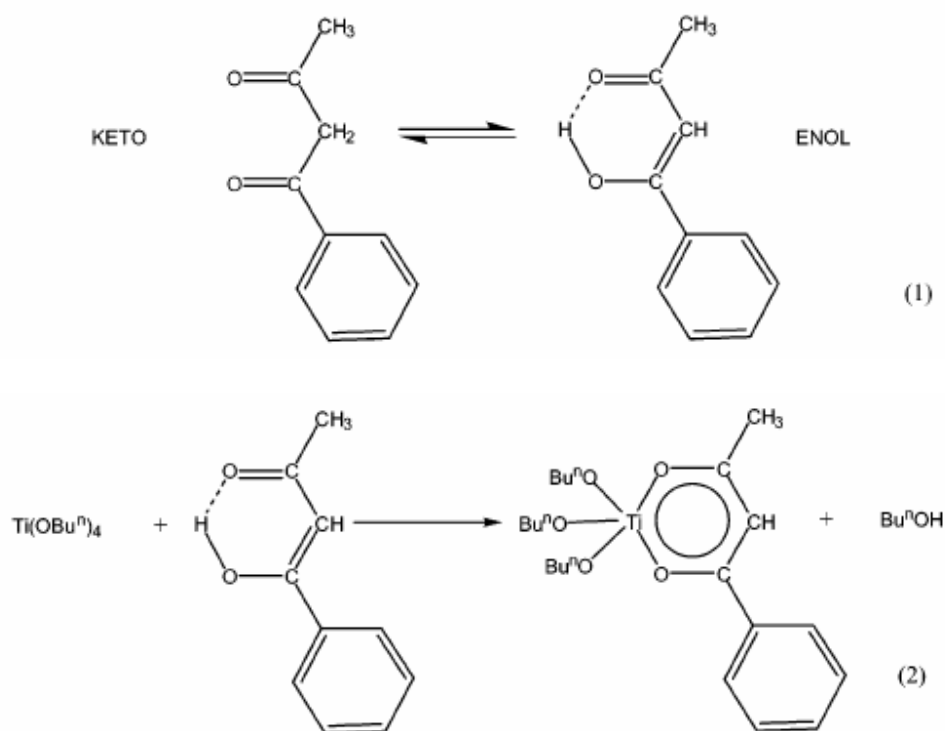


Figure 4. PL emission spectra of CdSe nanoparticles solution and the hybrid solution.



Subprogram 2 Nanohybrid materials⁴

We have demonstrated a synthetic route for preparing novel hybrid materials of P3HT/D-A linker/TiO₂. The chemical structure of the D-A linker was designed to contain three main parts: triethoxysilane group, alkyl spacer, and polymerizable thiophene ring. The preparation of the hybrid materials involves the formation of a self-assembled monolayer of D-A linker on the TiO₂ nanoparticles, followed by a surface-initiated electrochemical polymerization of 3-hexylthiophene.

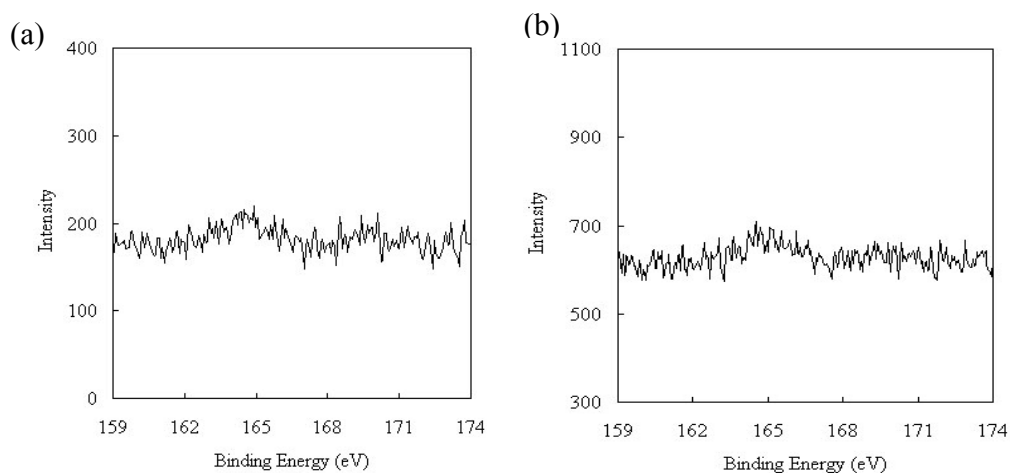
Table 1 shows the advancing water contact angles measured by FTA 125 (First Ten Ångstroms) on SAMs made by immersing TiO₂-coated ITO glass with D-A linkers bearing different alkyl spacer length. Obviously, the advancing contact angles increased with the increasing of the alkyl spacers. It clearly indicates that the advancing contact angles were nearly

independent of the immersion time in the range 45 to 180 min.

Table 1. Advancing water contact angles of **TEST**, **TESHT**, and **TESDT** SAMs on TiO₂ of different immersing time.

Samples	0min.	2min.	15min.	45min.	3 h
TEST	<5°	30.2°	36.0°	37.1°	40.8°
TESHT	<5°	51.7°	60.4°	64.7°	71.3°
TESDT	<5°	45.3°	59.5°	67.2°	75.0°

The amount of D-A linkers anchored on TiO₂ nanoparticles was determined by thermogravimetric analysis and was estimated to be 1.13, 1.51, and 1.54 % for **TEST**, **TESHT**, and **TESDT** SAMs, respectively. From the known surface area of TiO₂ particles (72.66 m² g⁻¹ determined by the BET method, Micrometer Tristar) and the amount of linker anchored, the average area occupied by one linker molecule was calculated to be 0.88, 1.31, and 1.72 nm² for **TEST**, **TESHT**, and **TESDT** SAMs, respectively. The different absorption behavior of the SAMs is attributed to the alkyl spacers in the linker molecules. While **TESHT** or **TESDT** SAM was fabricated, the long chains form an array dotted on the surface of the monolayer, this array causes a steric effect which obstructs the adsorption of more linker molecules on the TiO₂ surface. In the other word, the strength of the steric effect increased with the increase of the length of alkyl spacers. By the way, the weight increase in the TGA curves of **TESHT** and **TESDT** between 180 and 270 °C is may due to the partial oxidation of alkyl spacers. XPS spectra show that a peak at 164 eV was observed for every SAM modified TiO₂ substrate except the bare TiO₂ substrate. The signal at 164 eV was coming from the sulfur atom in thiophene rings. Combine the advancing water contact angle measurement, thermogravimetric analysis, and XPS spectra, we can presume that compact SAMs were formed on the surface of TiO₂.



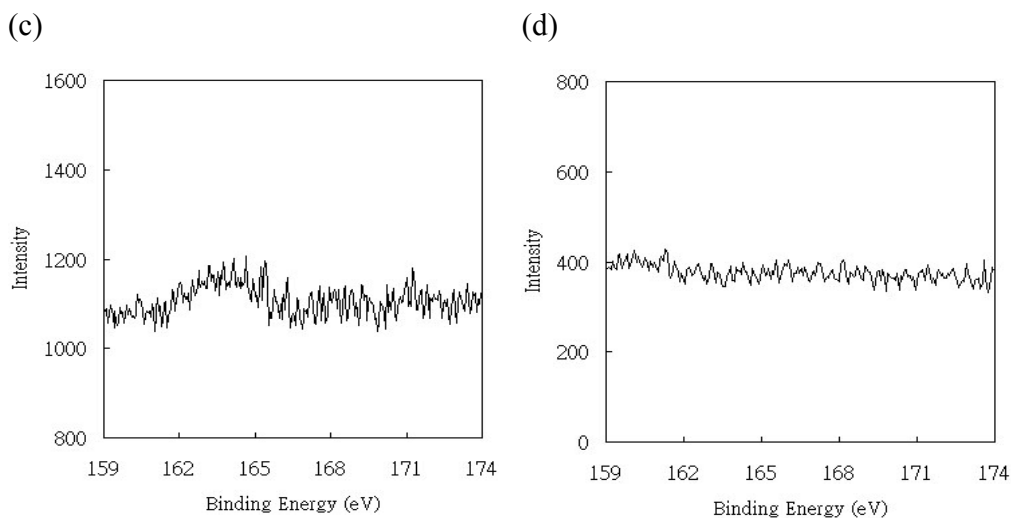


Figure 5. XPS spectra of (a) **TEST**, (b) **TESHT**, or (c) **TESDT** modified TiO_2 substrates, and (d) TiO_2 substrate.

Electrochemical polymerization of 3-hexylthiophene was carried out in a one-compartment three-electrode cell containing 0.05 M 3-hexylthiophene and 0.02 M Bu_4NBF_4 in anhydrous acetonitrile. After the reaction, the films were treated with ultrasound in THF twice and then in CHCl_3 twice. Figure 6 shows a strong adhesion of poly(3-hexylthiophene) to those substrates modified by **TEST**, **TESHT**, or **TESDT** when films were subjected to ultrasound in THF and CHCl_3 . This result further proved that the linkers chemically reacted with the Ti-OH group on TiO_2 surface to form Ti-O-Si bonds.

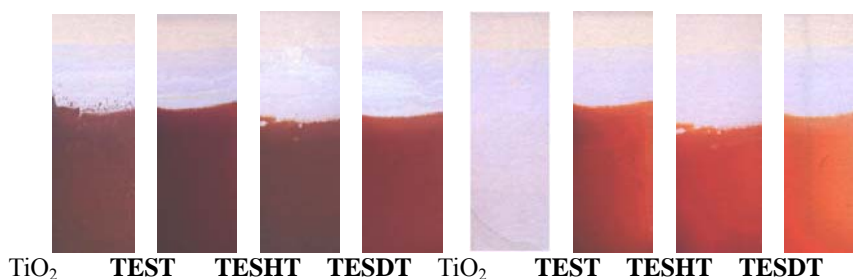


Figure 6. Left: Electrosynthesized P3HT films on TiO_2 , **TEST**, **TESHT**, and **TESDT** before treating with ultrasound in THF and CHCl_3 . Right: Electrosynthesized P3HT films on TiO_2 , **TEST**, **TESHT**, and **TESDT** after treating with ultrasound in THF and CHCl_3 .

UV-vis spectra (measured with Hitachi U-3410 Spectrophotometer.) of P3HT growing from **TEST**, **TESHT**, or **TESDT** modified TiO_2 substrates were showed in Figure 7. The maximum absorbance values (λ_{max}) were decreasing with increasing of the length of the alkyl spacers apparently. One possible reason is the resistance effect, which was caused by the alkyl spacers, formed a barrier to bring about interferences.

According to size-exclusion chromatography (using polystyrene as standards), the in-situ polymerized P3HTs growing from the **TEST**-, **TESHT**-, and **TESDT**-modified TiO₂ surface have $M_n = 48,300$, $42,600$, $31,400$, and $14,900$ g mol⁻¹, and polydispersity index = 3.04, 2.45, 2.40, and 2.35, respectively. This result can also demonstrate the presence of the resistance effect of alkyl spacer during electrochemical polymerization of P3HT. Although M_n was decreasing with increasing of alkyl spacer length, absorbance onset (λ_{edge}) did not shift apparently, as shown in Figure 7. It means that all in-situ polymerized P3HTs on **TEST**-, **TESHT**-, and **TESDT**-modified TiO₂ surface possess similar conjugated length even if they are much different in molecular weight.

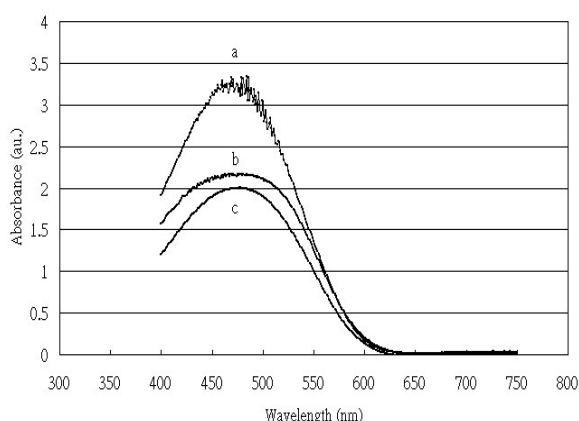


Figure 7. UV-vis spectra of P3HT propagating from (a) **TEST**, (b) **TESHT**, and (c) **TESDT** modified TiO₂ substrates.

Compared with GPC, TGA, and UV-vis measurements, the maximum absorbance values were not in proportion to the product of M_n and absorption densities. It could be explained by that the linkers were too compact to propagate P3HT chains from each linkers.

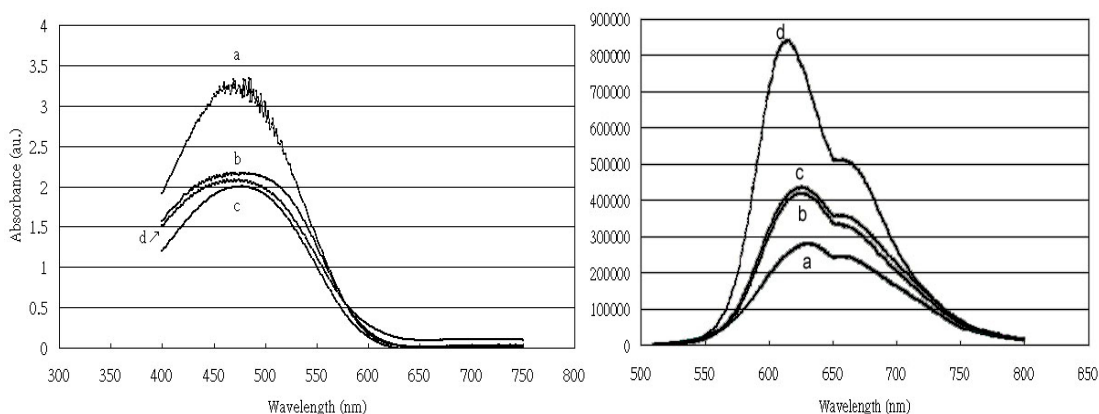


Figure 8. Left: UV-vis spectra of P3HT propagating from (a) **TEST**, (b) **TESHT**, or (c) **TESDT** modified TiO₂ substrates and (d) TiO₂ substrate. Right: Photoluminescence of P3HT films as above.

Figure 8 is the UV-vis and photoluminescence spectra (measured by Tau-3 fluorescence-lifetime system) of P3HT films. Although the UV-vis absorbance was decreasing, but the photoluminescence was increasing as the alkyl spacer length in the SAM molecules decreased. This is also due to the presence of resistance effect of alkyl spacers which formed a barrier to bring about interferences, thus raising difficulty of charge transportation. Compared with neat P3HT film growing from bare TiO₂ surface, the P3HT films growing from SAMs had much lower photoluminescence. It resulted from the phase separation between TiO₂ and P3HT, and therefore generated a much higher barricade to block off the channels of charge transfer. That is to say, the donor-acceptor linkers could avoid phase separation between TiO₂ and P3HT, and consequently promote the charge transfer efficiency of photoexcited electron-hole pairs in photovoltaic devices substantially.

Subprogram 3 Synthesis of self assemble conducting-insulation copolymer⁵

*Synthesis and morphology of poly(*p*-phenylene)-*b*-poly(2-vinylpyridine)*

Poly (1,3-cyclohexadiene)-*b*-poly (2-vinyl pyridine) (PCHD-PVP) copolymers were synthesized by sequential living anionic polymerization performed on a polymerization line constructed in this laboratory. The copolymerization reaction is carried out in THF solution at -78°C. For diblock copolymers, the addition sequence is as follows: CHD, initiator and finally VP monomer. Reaction schematic is shown in Figure 9.

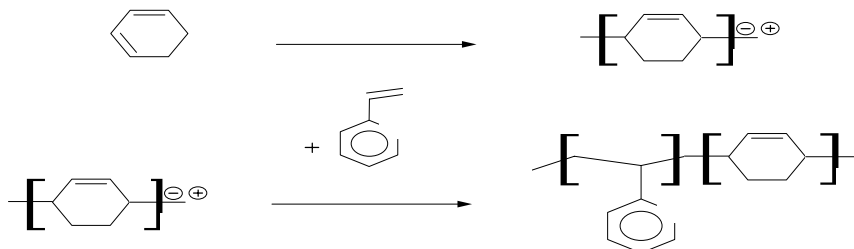


Figure 9. Reaction schematic of copolymerization of CHD and VP using anionic polymerization technique

GPC is used to measure the molecular weight of PCHD precursor and PCHD-PVP copolymer as shown in Figure 10 (a). PCHD homopolymers is synthesized with polydispersity (PDI) < 1.1. Block copolymer of PCHD-PVP can be synthesized upon the addition of VP monomers to the living PCHD anion solution. GPC measurement shows that some PCHD anions are terminated upon VP addition leading to a bimodal distribution of molecular weight. However, PCHD homopolymers can be removed from block copolymer PCHD-PVP by using a Soxhlet extraction method with cyclohexane as solvent. GPC measurement shows that the final molecular weight and PDI (PDI < 1.09) of PCHD-PVP as shown in Figure 10 (b).

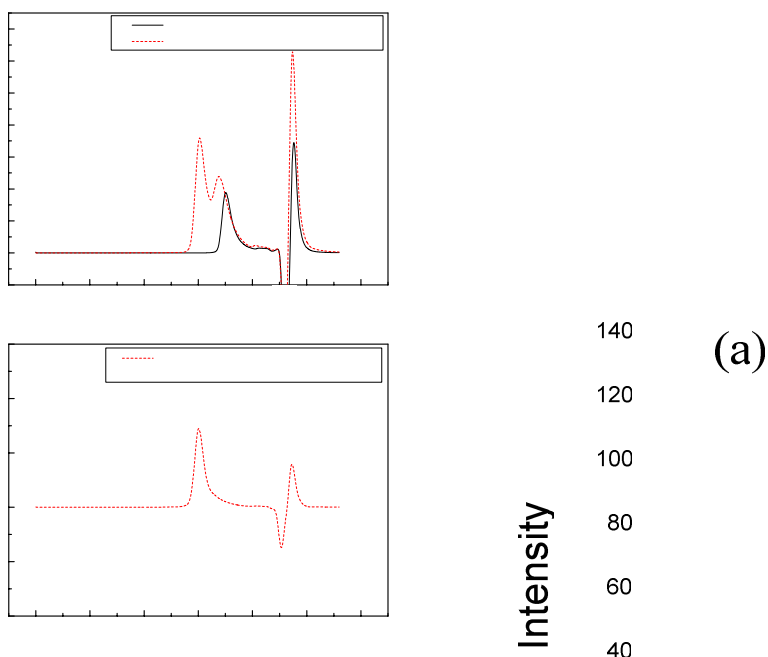


Figure 10. (a) GPC measurement of PCHD (solid line) and PCHD-PVP block copolymer (dashed line) before fractionation. (b) GPC measurement of PCHD-PVP block copolymer (dashed line) after fractionation.

The polymerization of 1,3-cyclohexadiene monomer can proceed in a 1,4- and 1,2- mode to give the structures shown in Figure 11.

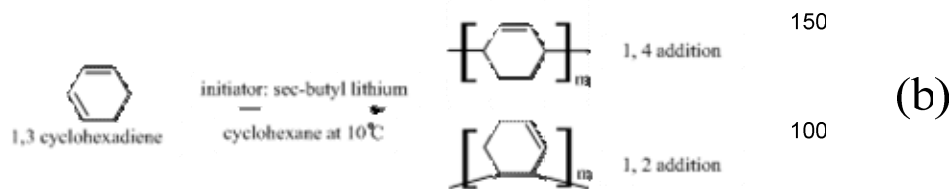


Figure 11. Two structural modes of PCHD.

The structural content between 1,4- and 1,2- mode of PCHD can be measured using ¹H-NMR as shown in Figure 12. From Figure 12, it is shown that the PCHD is synthesized in THF with molar ratio of 1,4 addition to 1,2 addition roughly equal to 86:14.

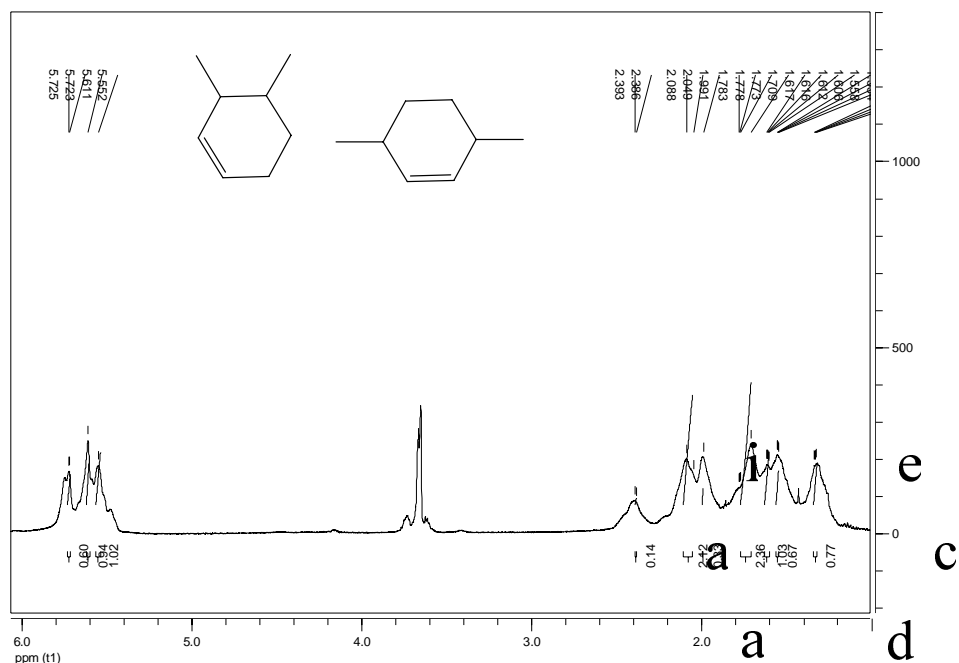


Figure 12. H-NMR of PCHD

The morphology of PCHD-PVP copolymers synthesized for this study was measured using transmission electron microscopy (TEM). To attain its equilibrium morphology, a bulk specimens of PCHD-PVP copolymers was annealed in a vacuum oven at 160°C for 3 days. A JEOL 1230 electron microscope operated at 120 KV was used to examine thin sections prepared from bulk specimens. Thin sections approximately 1000Å thick for TEM were obtained by ultramicrotomy with a diamond knife on a Leica Ultracut microtome. In order to visualize a specimen in the TEM one must have contrasting regions of electron transparency and electron opacity. Thin section of the specimens is exposed to iodide vapor for 12 hours in order to stain PVP region. For PCHD_f-PVP_{1-f} with $f = 0.63$ and weight-average molecular weight = 14,000, TEM micrograph shows self-assembled morphology of the copolymer with lamellar structure (Figure 13) of long spacing of roughly 50nm.

a

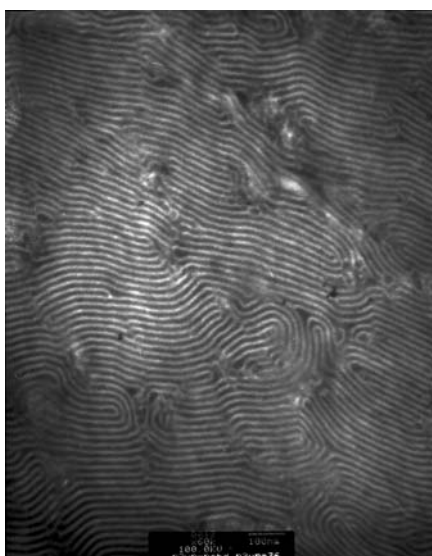


Figure 13. TEM micrograph of PCHD_f-PVP_{1-f} with $f = 0.63$ and $M_w = 14,000$. PVP region stained by I₂ appear dark in TEM micrograph.

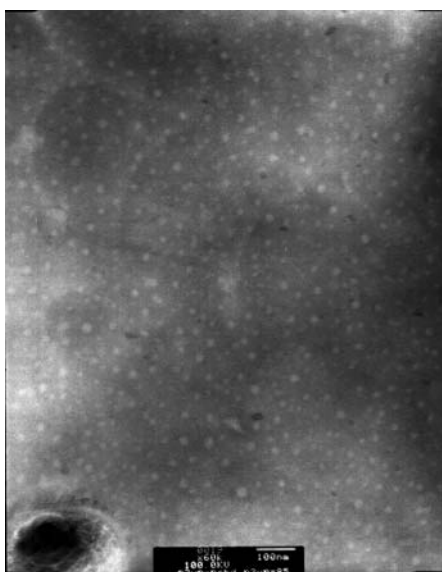


Figure 14. TEM micrograph of PCHD_f-PVP_{1-f} with $f = 0.15$ and $M_w = 100,000$. PVP region stained by I₂ appear dark in TEM micrograph.

For PCHD_f-PVP_{1-f} with $f = 0.15$ and weight-average molecular weight = 100,000, TEM micrograph shows self-assembled morphology of the copolymer with spherical structure as shown in Figure 14.

The conversion reaction of PCHD to PPP is shown as follows:



Figure 15. Schematic of conversion reaction of poly (1,3 cyclohexadiene) (PCHD) to poly (para phenylene) (PPP).

The dehydrogenation reaction is carried out by refluxing PCHD-PVP copolymer with chloranil and xylene as solvent. The reflux condition is maintained for 48 hours. The mixture was then cooled and filtered to obtain a brown solid product. The product was then rigorously washed and extracted using a Soxhlet apparatus with solvent wash. PPP polymer was then obtained after oven drying. Figure 16 shows NMR of PPP to indicate the conversion of PPP. In general, more than 90% of PCHD is converted to PPP using the above method.

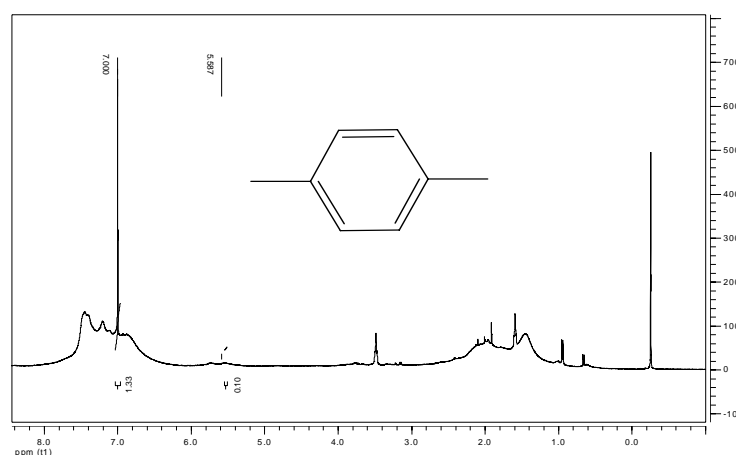
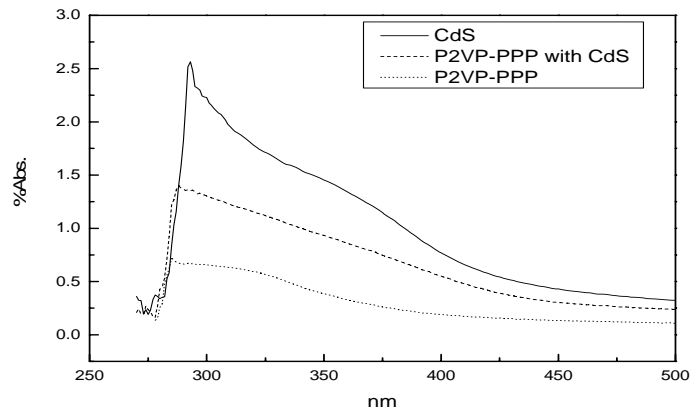


Figure 16. H-NMR of PPP

The CdS nanoparticle was in-situ formed on PPP-PVP in solution. The film of CdS-PPP-PVP was spin coated on quartz substrates. The bandgap of copolymer was determined from UV spectra. The CdS containing copolymer. (P2VP₈₆-PPP₁₄; 86% volume ratio P2VP, 14% volume ratio PPP) exhibits a lower bandgap (2.88eV) than that of neat polymer P2VP₈₆-PPP₁₄ (3.29eV) (Figure 17). The results indicate a higher solar light absorption for CdS containing copolymer. The photoluminescence of CdS containing copolymer has exhibited a lower PL intensity than that of neat copolymer (Figure 18). The reduced PL intensity may result from a higher electron transport in the CdS containing copolymer.

(a)



(b)

Item	PPP ₈₆ -PPP ₁₄	PPP ₈₆ -PPP ₁₄ +CdS
Max (nm)	293	288
Edge (nm)	377	431
Band Gap (eV)	3.29	2.88

Figure 17. (a) UV-Vis measurement of pure CdS, PVP-PPP and PVP-PPP+CdS hybrid. (b) Comparison of maximum absorption, edge absorption and band gap between PPP-PVP and PPP-PVP+CdS

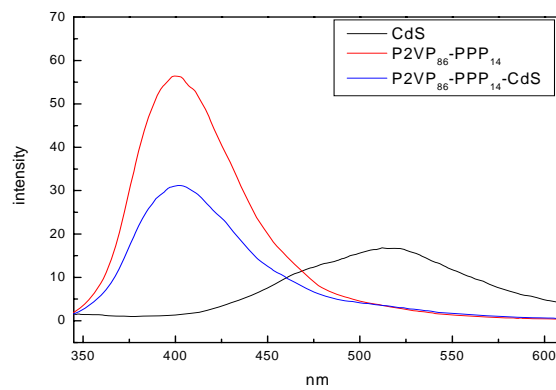
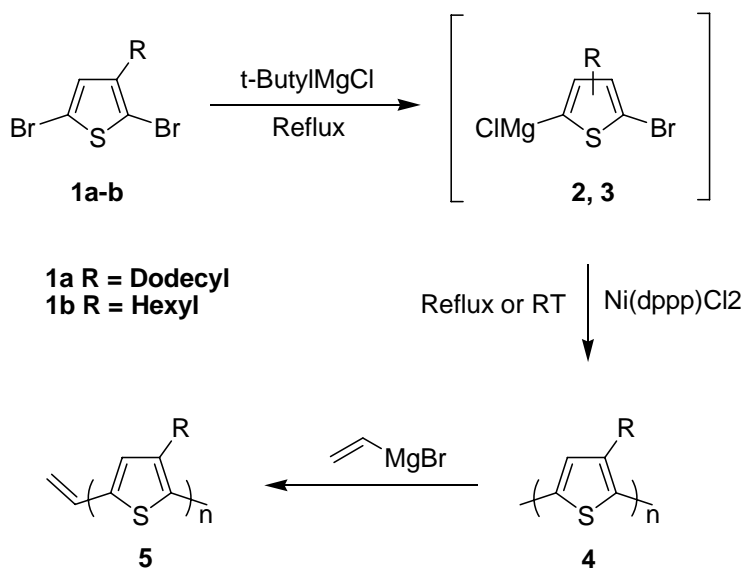


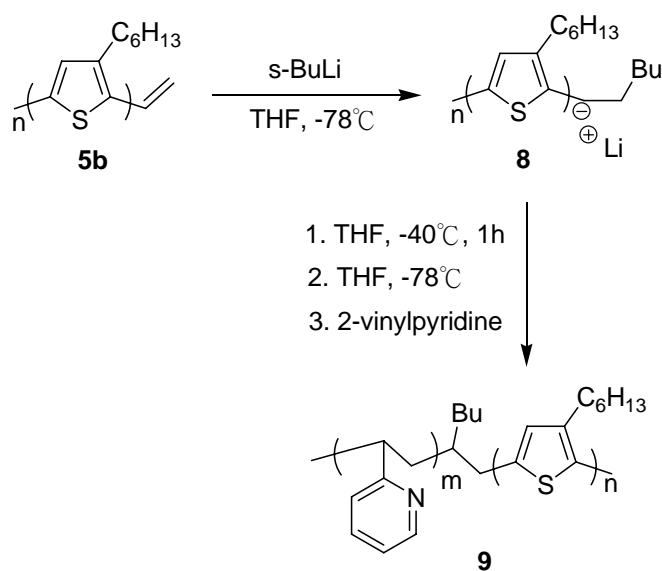
Figure 18. PL Spectra of P2VP₈₆-PPP₁₄(top line), P2VP₈₆-PPP₁₄-CdS (middle line), CdS (bottom line)

Synthesis of poly(3-hexylthiophene)-b-poly(2-vinylpyridine)

The charge mobility of polythiophene is at least one order higher than that of poly-p-phenylene, so we also study the polythiophene copolymer system. We have synthesized poly(3-hexylthiophene)-b-poly(2-vinylpyridine) using anionic polymerization via the following Scheme 3 and Scheme 4.



Scheme 3. Synthesis of poly(3-alkylthiophene) with terminal vinyl group.



Scheme 4. Synthesis of poly(3-hexylthiophene)-b-poly(2-vinylpyridine) via anionic polymerization

The chemical structure of copolymer has confirmed by NMR and UV. Their molecular weight was determined by GPC and MALDI-TOF. It is interesting to find that the λ_{max} of UV spectra (Figure 19) and PL spectra (Figure 20) has blue shifted about 40 nm and 14 nm respectively for copolymer as compared with the spectra of blend of each polymer. The results may be due to the decreasing in conjugated length of polythiophene when it was connected to insulating polyvinyl pyridine. .

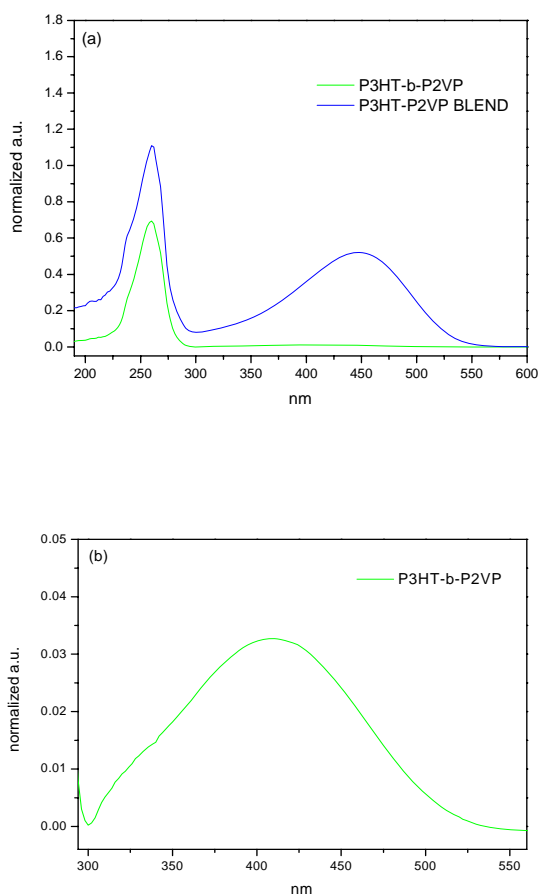


Figure 19. (a) normalized UV-Vis absorption spectra of P3HT, P2VP, P3HT-b-P2VP and P3HT/P2VP blended, (b) enlarged portion of P3HT-b-P2VP ranged from 300 ~ 550 nm.

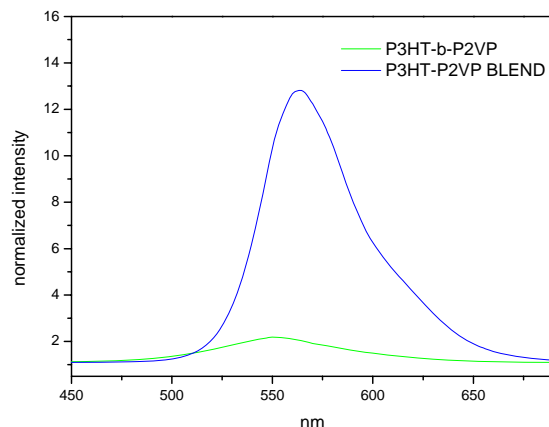


Figure 20. normalized photoluminescence spectra of P3HT, P2VP, P3HT-b-P2VP and P3HT/P2VP blended

Subprogram 4. Mechanisms of charge separation and transport in organic/inorganic hybrid materials

We have finished setting up several measurement systems as shown in Figure 21 required in this project to study the mechanisms of charge separation and charge transport, including (a) standard solar simulator (b) organic/inorganic hybrid photovoltaic device *I-V* characteristics measurements. (c) Internal and external quantum efficiency measurement. (d) Temperature-dependent steady-state photoluminescence system. (e) Temperature-dependent time-resolved photoluminescence system. (~ 100 ps).

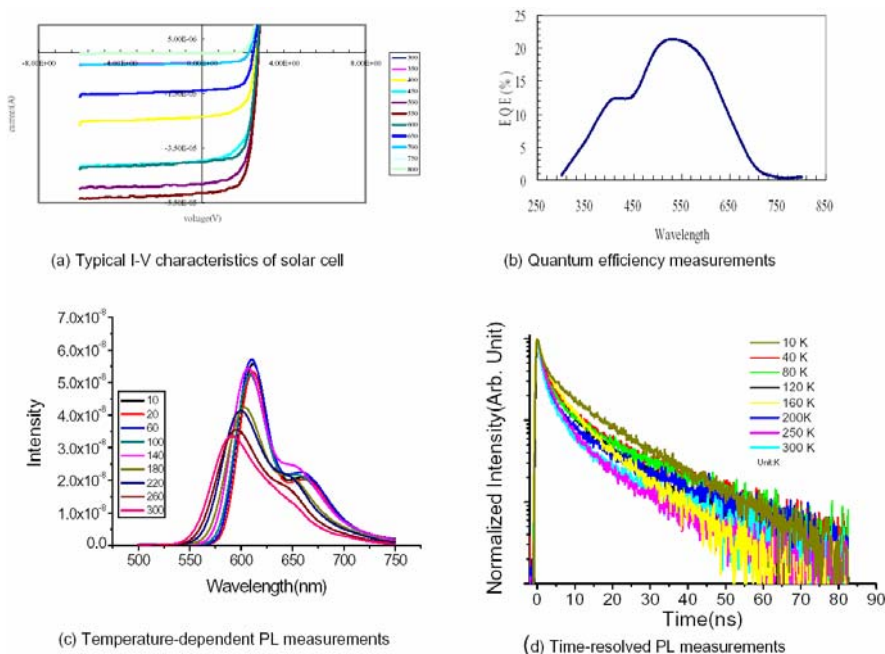


Figure 21. (a) *I-V* characteristics of solar cell (b) Quantum efficiency measurements (c) Temperature-dependent PL measurements (d) Time-resolved PL measurement

Sample preparation

The MEH-PPV/CdSe hybrid composite materials as shown in Figure 22 have been prepared by varying the CdSe nanoparticle concentrations ratios. The active layer with a thickness of 200 nm was deposited on the indium tin oxid(ITO) coated glass substrate with sheet resistance $10\Omega\text{-cm}$. The Al electrode was then deposited on the top of the active layer by thermal evaporator with a pressure of at 5×10^{-6} torr.

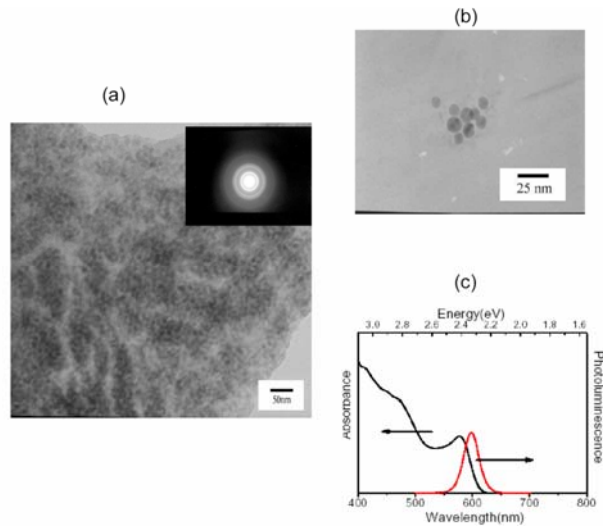


Figure 22 (a) The TEM image of MEHPPV/CdSe nanocrystal hybrid system . (b) The TEM image of CdSe nanocrystals. (c) Absorption and PL spectra of CdSe nanocrystals in (b).

Absorption enhancement and PL quench

Figure 23(a) shows the absorption and PL spectra of MEHPPV/CdSe nanocrystal hybrid materials with different compositions. It is shown that as the concentration of CdSe nanocrystals increases, the enhancement of absorption coefficients and the quench of PL intensities are obviously observed, indicating that significant charge separation occurs at the polymer/nanocrystal interfaces with an electron on the nanocrystal and a hole on the polymer. Figure 23(b) shows the luminescence decay curves of MEHPPV/CdSe nanocrystal thin films with various compositions. The PL decay time decreases as the concentration of CdSe nanocrystals increases, indicating that electron transfer from an excited PPV block to a CdSe nanoparticle occurs efficiently (Table 2).

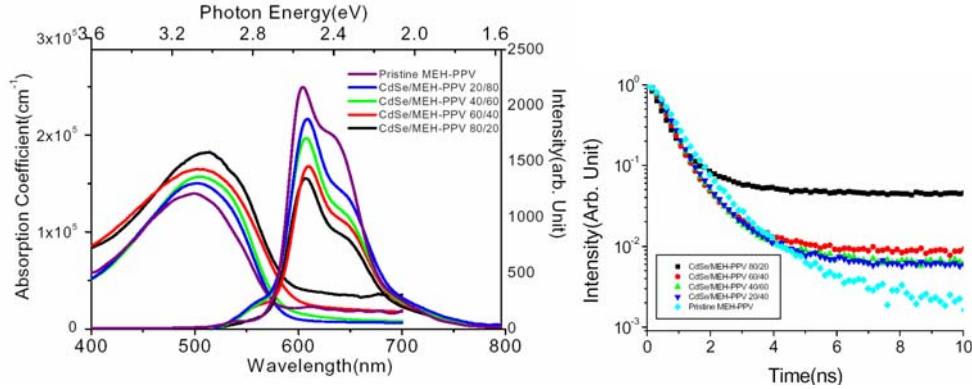


Figure 23 (a) Absorption and PL spectrum of MEHPPV/CdSe hybrid materials (b) Time-resolved PL spectra of MEHPPV/CdSe hybrid materials

Table 2. Decay time of different ratio of CdSe/MEHPPV hybrid materials

Sample number	Cdse/MEH-PPV ratio	Life Time (ns)
Sample 1	Pristine polymer	$\tau_1=0.78$
Sample 2	20/80	$\tau_1=0.68$
Sample 3	40/60	$\tau_1=0.66$
Sample 4	60/40	$\tau_1=0.56, \tau_2=0.63$
Sample 5	80/20	$\tau_1=0.53425, \tau_2=3.3$

Exciton dynamics in the polymer/nanocrystal hybrid materials

In order to understand the fundamental charge separation mechanism in the polymer/nanocrystal hybrid materials, we carried a series of temperature dependent steady-state and time-resolved photoluminescence experimental studies. Figure 24(a) shows the temperature-dependent PL spectra of the MEHPPV/CdSe nanocrystal (40:60 %wt) thin film. The redshift induced with decreasing temperature has been observed as the results of an increase in the effective conjugation length while temperature decreases due to the reduction of torsion motions. Such an effect increases the delocalization of the π electrons and acts a decrease of the band-gap size. The full width at half maximum (FWHM) of the PL zero-phonon peak (0-0) decreases monotonically with decreasing temperature. The increase of effective conjugation length with decreasing temperature is also reflected from the longer PL decay time as shown in Figure 24(b). In addition, the intensity of the nth-order PL peak related to that of the zero-phonon

peak by the Huang-Rhys equation $I_n = \frac{S^n}{n!} I_0$ is also shown in Figure 24(d). The decreasing

Huang-Rhys parameter S with decreasing temperature is the result of increased conjugation and exciton delocalization over more repeat units of the polymer chain, made possible by the freezing out of molecular torsions and other low-frequency vibration modes that distort the polymer from planarity and disrupt conjugation.

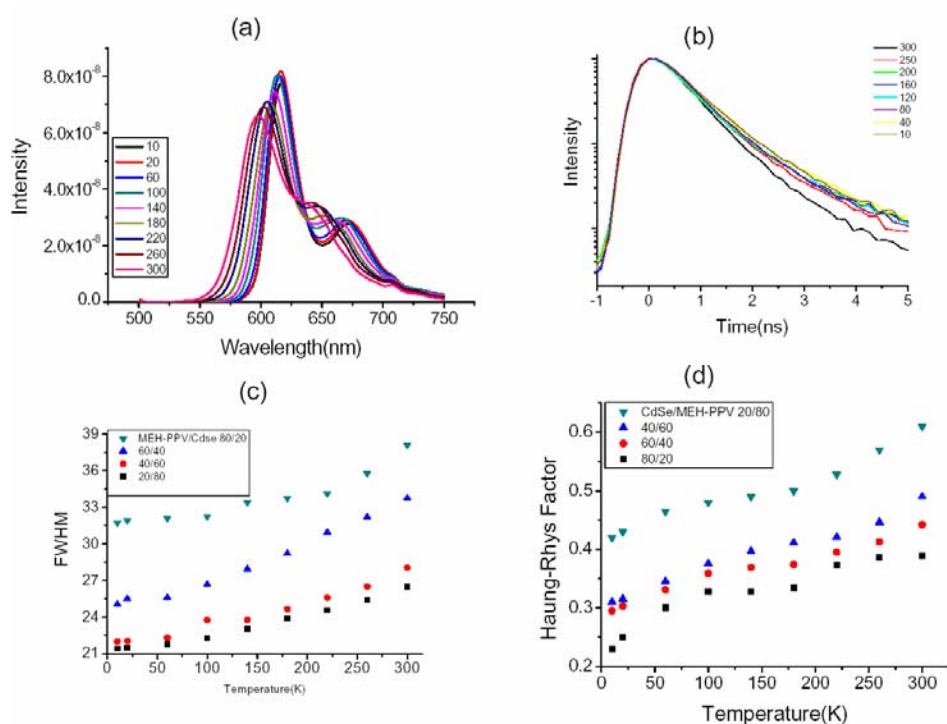


Figure 24. (a) Temperature-dependent PL spectra of MEHPPV/CdSe hybrid (40:60 wt%) (b) Temperature-dependent time-resolved PL (c) Temperature-dependent FWHM of MEHPPV/CdSe hybrids with different ratios (d) Temperature-dependent Huang-Rhys factor for MEHPPV/CdSe hybrids with different ratios

Next, while we varied the composition of MEHPPV/CdSe thin films, we found the FWHM (0-0) and the Huang-Rhys factors of the thin films decrease with the increasing CdSe nanocrystal concentration at all measured temperature, indicating that an increase of effective conjugation length and delocalization of the π electrons occurs when more nanocrystals are included in the polymer matrix. We propose a model to interpret the results. As the CdSe nanocrystal concentration increases, the torsion motion of the polymer units is spatially limited by the CdSe nanocrystals due to their heavier mass. This relatively enhances the coplanar features of polymer, leading to the increase of the effective conjugation length, which is reflected from the redshift of the PL spectra with the increasing nanocrystal concentration as shown in Figure 25. This result reveals the information that in the polymer/nanocrystal hybrid materials, the role of nanocrystals not only provides medium for efficient charge separation at the interface but also leads to the increase the effective conjugation length in the polymer, which could be beneficial for hole transport within the polymer chain. This result is a very preliminary one and is a promising starting point for further studies dealing with its optimization.

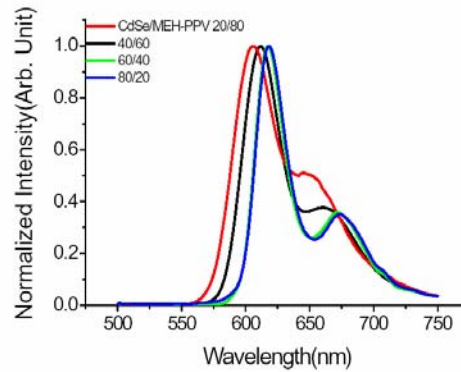


Figure 25. PL spectra of MHEPPV/CdSe hybrid systems shift toward the lower energy as the concentration of CdSe increases

Preliminary Studies of Device Fabrications

A solar cell device based on the polymer/nanocrystal hybrid material was fabricated and the photo-response of the solar cell is shown in Figure 26. It was shown that the short-circuit photocurrent enhances with increasing CdSe/MEHPPV ratio, consistent with a higher charge separation efficiency. Although the fill factor for this device is relatively high (37.5 %), the power conversion efficiency ($< 0.1\%$) for the device is still very low. Since the performance of a solar cell depends strongly both on the charge separation and on the charge transport, we believed the low power conversion efficiency at this stage is due to the poor transport path for carriers, although the excellent charge separation efficiency was found in the MEHPPV/CdSe nanocrystal interface as mentioned above. Further optimization for device fabrication conditions is required to improve the device performance.

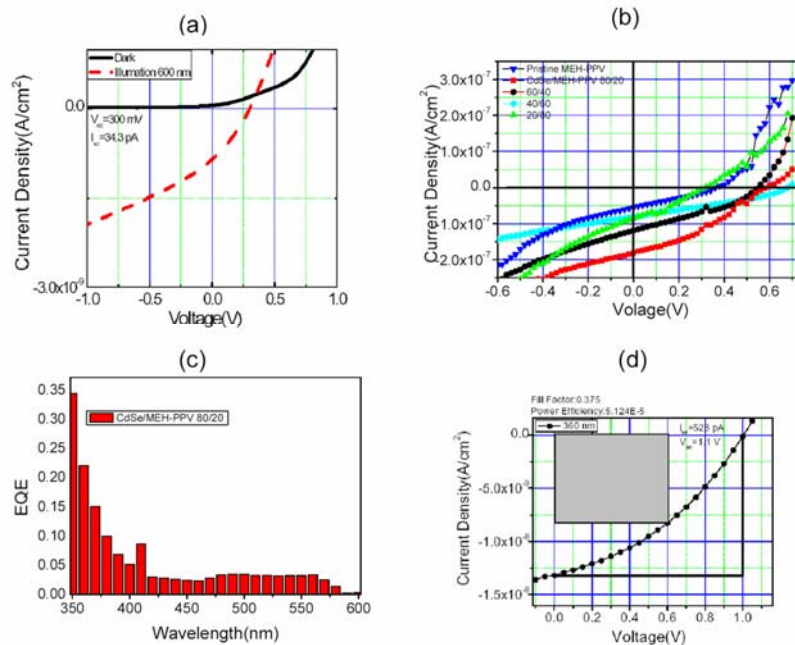


Figure 26. (a) I-V characteristics of pristine MEHPPV (b) I-V characteristics of MEHPPV/CdSe nanoparticles with different ratios (c) External quantum efficiency of the sample (MEHPPV/CdSe 20:80). (d) The fill factor(0.35) in (c).

References

1. S. E. Shaheen et al. *MRS Bulletin*, **2005**, 30, 10.
2. D. V. Talapin, A. L. Rogach, A. Kornowski, M. Haase, H. Weller, *Nano Lett.* **2001**, 1, 207.
3. M. S. M. Saifullah, K. R. V. Subramanian, E. Tapley, D. J. Kang, M. E. Welland, and M. Butler, *Nano Lett.*, **2003**, 3, 1587.
4. L.Y. Wang, H.J. Cheng and W.F. Su, "Photovoltaic cells fabricated from hybrid materials of TiO₂/molecular linker," present in 20th European PVSEC, 6-10 June 2005, Barcelona, Spain.
5. C.J. Kao, C.A. Dai, C.C. Ho and W.F. Su, "Patterning Nanoparticles in self-assembled conducting/insulating block copolymer," present in 2004 MRS Fall Meeting, L5.7, Boston, USA.
6. W.F. Su, C.C. Ho, C.A. Dai, "Block copolymer containing nanoparticles, electron transporting material and photoelectric device employing the same," Taiwan patent filed 2005. 5.27.